

Effect of Sm doping into CuInTe2 on cohesive energy before and after light absorption

Tai Wang(王泰), Yong-Quan Guo(郭永权)†, and Cong Wang(王聪)

Citation: Chin. Phys. B, 2021, 30 (**4**): 043101. DOI: 10.1088/1674-1056/abd167
Journal homepage: http://cpb.iphy.ac.cn; http://iopscience.iop.org/cpb

What follows is a list of articles you may be interested in

Influence of sub-bandgap illumination on space charge distribution in CdZnTe detector

Rongrong Guo(郭榕榕, Jinhai Lin(林金海), Lili Liu(刘莉莉), Shiwei Li(李世韦), Chen Wang(王尘), Feibin Xiong(熊飞兵), and Haijun Lin(林海军)
Chin. Phys. B, 2021, 30 (**3**): 036101. DOI: 10.1088/1674-1056/abc67e

CdS/Si nanofilm heterojunctions based on amorphous silicon films: Fabrication, structures, and electrical properties

Yong Li(李勇), Peng-Fei Ji(姬鹏飞), Yue-Li Song(宋月丽), Feng-Qun Zhou(周丰群), Hong-Chun Huang(黄宏春), and Shu-Qing Yuan(袁书卿)
Chin. Phys. B, 2021, 30 (**2**): 026101. DOI: 10.1088/1674-1056/abc15e

Correlation between electronic structure and energy band in Eu-doped $CuInTe_2$ semiconductor compound with chalcopyrite structure

Tai Wang(王泰), Yong-Quan Guo(郭永权), Shuai Li(李帅)
Chin. Phys. B, 2017, 26 (**10**): 103101. DOI: 10.1088/1674-1056/26/10/103101

Magic wavelengths for the $7s_{1/2}$-$6d_{3/2,5/2}$ transitions in Ra^+

Xiao-Mei Wu(吴晓梅), Cheng-Bin Li(李承斌), Yong-Bo Tang(唐永波), Ting-Yun Shi(史庭云)
Chin. Phys. B, 2016, 25 (**9**): 093101. DOI: 10.1088/1674-1056/25/9/093101

Calculations on polarization properties of alkali metal atoms using Dirac-Fock plus core polarization method

Tang Yong-Bo, Li Cheng-Bin, Qiao Hao-Xue
Chin. Phys. B, 2014, 23 (**6**): 063101. DOI: 10.1088/1674-1056/23/6/063101

Effect of Sm doping into $CuInTe_2$ on cohesive energy before and after light absorption

Tai Wang(王泰), Yong-Quan Guo(郭永权)†, and Cong Wang(王聪)

School of Energy Power and Mechanical Engineering, North China Electric Power University, Beijing 102206, *China*

(Received 19 October 2020; revised manuscript received 27 November 2020; accepted manuscript online 8 December 2020)

The effects of Sm doping into $CuInTe_2$ chalcopyrite on the cohesive energy before and after light absorption are systematically investigated by the empirical electron theory (EET) of solids and molecules. The results show that the static energy of $CuIn_{1-x}Sm_xTe_2$ decreases with Sm content increasing due to the valence electronic structure modulated by doping Sm into $CuIn_{1-x}Sm_xTe_2$. The calculated optical absorption transition energy from the static state to the excited energy level in $CuIn_{1-x}Sm_xTe_2$ accords well with the experimental absorption bandgap of $CuIn_{1-x}Sm_xTe_2$. Moreover, it is found that the energy bandgap of $CuIn_{1-x}Sm_xTe_2$ is significantly widened with Sm content increasing due to its special valent electron structure, which is favorable for enhancing the light absorption in a wider range and also for the potential applications in solar cells.

Keywords: $CuIn_{1-x}Sm_xTe_2$, empirical electron theory (EET), light absorption bandgap, hybridization energy

PACS: 31.15.bu, 61.72.uj, 42.70.Qs, 71.15.Nc **DOI:** 10.1088/1674-1056/abd167

1. Introduction

The I–III–VI_2 chalcopyrite is investigated for its potential applications in nonlinear optical device, semiconductor laser device, and solar cells[1–6] due to its excellent photoelectric properties such as large absorption coefficient, direct bandgap, large nonlinear susceptibility in the infrared region.[7–11] The conversion efficiency η of Cu(In, Ga)(Se, S)$_2$ in solar cell with thin-film absorber layer has reached up to 22.6%.[10] However, single phase Cu(In,Ga)(Se,S)$_2$ is not easily prepared due to its composition deviation in the synthesizing process, and causes the impurities to form. Owing to the existence of toxical p-type CdS in Cu(In,Ga)Se_2 thin-film solar cells, its potential application is limited. The $CuInTe_2$ has a direct bandgap of 1.06 eV at room temperature,[12] which matches the light absorption bandgap of solar energy conversion. Therefore, $CuInTe_2$ is predicted to have stronger quantum confinement effect and larger Bohr radius of exciton than the CuIn(S/Se)$_2$ due to the covalent property of Te.[7]

The double layers Cu(In, *R*)Te_2/Cu(In, *R*)Te_2 (*R* = rare earth) are designed for controlling the charge transport by modulating the valent state of the rare earth, *e.g.* Ce^{4+} for p-type and Eu^{2+} for n-type,[12–15] which can simplify the synthesis technology from three-layer ZnO/CdS/CIGS to two-layer Cu(In, *R*)Te_2/Cu(In, *R*)Te_2. Since the rare earth element has an excellent light transmission, it can be used to replace the transparent ZnO front electrode layer. After the rare earth element, which has specific 4f electronic structure and unique optical properties such as subsequent emission light at long wavelength and high quantum efficiencies of absorption, is doped into a semiconductor, its luminescent and fluorescent properties can be enhanced.[16–18] Sm is usually in two kinds of valence states, *i.e.* Sm^{2+} and Sm^{3+}. Sm ion substituted for In in $CuInTe_2$ might adjust the charge transport type of semiconductor (Sm^{2+} for n type). Thus, $CuIn_{1-x}Sm_xTe_2$ chalcogenide might be developed into a promising absorber material for new-generation solar cells due to its low toxicity and good optical property.

In this study, the empirical electron theory (EET) is used to investigate the effect of Sm doped into $CuInTe_2$ on the cohesive energy before and after light absorption. The calculation of EET is very simple without any integral and differential calculations, and the number of its various parameters are much less than those of the other approaches such as the first principle and molecular field theory. The essential mechanism of light absorption can be revealed by the correlation between the properties and valence electron structure.

2. Calculation methods

The EET, which is based on Pauling's valence electron theory and quantum theory, consists of three hypotheses and a bond length difference method (BLD).[15,19–27]

Hypothesis 1 The electronic configurations of the static state (h) and the excitation state (t) are based on the observed photoelectronic energy spectra.[28] The involved electrons are the lattice electron n_l (⏀ or ⏁) in lattice spaces, the dumb-pair electron n_Y (‖) in atomic inner shells, the 3d magnetic electron m^{3d} (↑), the valence electrons n_c (•) in s, p, and d orbitals and equivalent d electron (•) transiting from d orbit to s or p orbit; and the total electrons n_T ($n_c + n_l$). The single-bond radius $R(l)$ is also defined in Refs. [28,29].

†Corresponding author. E-mail: yqguo@ncepu.edu.cn

© 2021 Chinese Physical Society and IOP Publishing Ltd

Hypothesis 2 According to the state superposition principle of quantum mechanics, the σ-th hybridization state is superposition of h state and t state, the hybridization states are discontinuous. A parameter of K is introduced for calculating the proportion $C_{\rm h}$ for h state and $C_{\rm t}$ for t state.[30,31]

The σ-th hybridization state is given by

$$C_{{\rm t}\sigma} = \frac{1}{K_\sigma^2+1}, \quad C_{{\rm h}\sigma} = 1 - C_{{\rm t}\sigma}, \tag{1}$$

$$K_\sigma = \frac{\tau' l' + m' + n'}{\tau l + m + n} \sqrt{\frac{l'+m'+n'}{l+m+n}} \frac{l \pm \sqrt{3m} \pm \sqrt{5n}}{l' \pm \sqrt{3m'} \pm \sqrt{5n'}}, \tag{2}$$

where the numbers of s, p, d valence electrons correspond, respectively, to l, m, n for h state and l', m', n' for t state; τ and τ' are 1 for the valence electron and 0 for the lattice electron in s orbit.

The numbers of various electrons N_σ can be calculated from $N_\sigma = C_{\rm h}N_{\rm h} + C_{\rm t}N_{\rm t}$ where $N_{\rm h}$ and $N_{\rm t}$ are the number of electrons in h state and t state, respectively.

Hypothesis 3 Pauling's equation is modified for calculating accurately the covalent bond length $D_{uv}(n_\alpha)$ between u and v atoms, which is expressed as

$$D_{uv}(n_\alpha) = R_u(l) + R_v(l) - \beta \log n_\alpha \quad (\alpha = A, B, \ldots, N), \tag{3}$$

where $R_u(l)$ and $R_v(l)$ are single bond radii of u and v atoms, respectively, the third term on the right-hand side denotes the effect of electron cloud overlap between u and v atoms, which induces the u–v bond length to elongate or shrink along the bonding direction; the coefficient β denotes the ability of electronic clouds to overlap each other, and the value of β is determined to be 0.6 for metal and alloy and 0.71 for the nonmetal in Pauling's valence and bond theory. The n_α denotes the number of covalent electron pairs in the α-th u–v bond. In the EET, modification is done according to the maximum of n_α as shown below:[28]

$$\beta = \begin{cases} 0.71\ \text{Å}, & n^M < 0.25 \text{ or } n^M > 0.75, \\ 0.6\ \text{Å}, & 0.3 \le n^M \le 0.70, \\ 0.71\ \text{Å} - 2.2\varepsilon\ \text{Å}, & n^M = 0.25 + \varepsilon \text{ or } n^M = 0.75 - \varepsilon, \end{cases} \tag{4}$$

with $0 < \varepsilon < 0.05$.

BLD: According to hypothesis III, the shortest bond length $D_{uv}(n_A)$ should be written as

$$D_{uv}(n_A) = R_u(l) + R_v(l) - \beta \log n_A. \tag{5}$$

Then we have

$$D_{\rm st}(n_\alpha) = R_{\rm s}(l) + R_{\rm t}(l) - \beta \log n_\alpha, \tag{6}$$

for the other bond lengths $D_{\rm st}(n_\alpha)$, $\alpha = B, C, \ldots, N$.

From Eqs. (5) and (6), we have

$$\lg \frac{n_\alpha}{n_A} = \lg r_\alpha = [D_{uv}(n_A) - D_{\rm st}(n_\alpha) - R_u(1) - R_v(1) + R_{\rm s}(1) + R_{\rm t}(1)]/\beta, \tag{7}$$

where $r_\alpha = n_\alpha/n_A$ and β are checked by Eq. (4). The calculation of n_A can be found in Ref. [29]. The theoretical bond length $\overline{D}_{uv}(n_\alpha)$ is estimated from $n_\alpha = r_\alpha n_A$ and Pauling's equation

$$\overline{D}_{uv}(n_\alpha) = R_u(l) + R_v(l) - \beta \log n_\alpha. \tag{8}$$

The bond length difference $|\Delta D| = |\overline{D}_{uv}(n_\alpha) - D_{uv}(n_\alpha)|$ is taken as a criterion for selecting the reasonable hybrid state. In general, $|\Delta D|$ is not more than 0.05 Å.

In this study, the 4b crystal position is disorderedly occupied by In and Sm in unit cell of $CuIn_{1-x}Sm_xTe_2$, In and Sm are taken as a kind of atom M at 4b site, *i.e.*, $M = (1-x)\cdot{\rm In} + x\cdot{\rm Sm}$. The average model is used to calculate the numbers of various electrons and averaged single bond radius as listed below:

$$n_{\rm ele} = x n_{\rm ele}^{\rm Sm} + (1-x) n_{\rm ele}^{\rm In}, \tag{9}$$

$$R_{\rm avg}(l) = x R_{\rm Sm}(l) + (1-x) R_{\rm In}(l), \tag{10}$$

where $n_{\rm ele}$, $n_{\rm ele}^{\rm Sm}$, $n_{\rm ele}^{\rm In}$ (ele = s, p, d, c, l, T, Y) donate the numbers of various electrons and the single bond radii are donated by $R_{\rm avg}(l)$ for M, $R_{\rm Sm}(l)$ for Sm, and $R_{\rm In}(l)$ for In.

The cohesive energy of intermetallic compound follows an equation as given below[31–35]

$$\overline{E_{\rm C}^0} = \sum\nolimits_\alpha \overline{B}_\alpha \frac{I_\alpha n_\alpha}{D_{(n_\alpha)}} \overline{F}_\alpha + \overline{B}_{\rm l} \frac{n_{\rm l}}{\overline{D}_{(n_{\rm l})}} f' + b_u a m^{3{\rm d}} - b_u C W + b_v a m^{3{\rm d}} - b_v C W, \tag{11}$$

where $\overline{B}_\alpha$ refers to the shielding coefficient along the α-th u–v bond, $\overline{B}_\alpha = \sqrt{b_u b_v}$, with b_u and b_v being the shielding coefficient of u and v atoms; b is defined as $b = 313.95/(n - 0.36\delta)$ (kcal·Å/mol) with $n = 1, 2, 3, 4, 5, 8$ or 13, $\delta = 2, 1, 0$; $\overline{F}_\alpha$ represents the bonding capability of covalent electron of the α-th u–v bond, $\overline{F}_\alpha = \frac{1}{2}(f_u + f_v)$, where $f = \sqrt{\alpha} + \sqrt{3\beta} + g\sqrt{5\gamma}$, $\alpha = n_{\rm s}/n_{\rm T}$, $\beta = n_p/n_{\rm T}$, $\gamma = n_d/n_{\rm T}$; I_α is the number of equivalent bonds; $\overline{B}_{\rm l} = \sqrt[m+n]{b_u^m b_v^n}$; $\overline{D} = \sum I_\alpha D_{(n\alpha)}/\sum I_\alpha$ is the weighted average of all bond distances; $f' = \sqrt{2\alpha'}$ is the bonding capability of lattice electrons, and $\alpha' = n_{\rm l}/n_{\rm T}$, with $n_{\rm T}$ being the total number of valence electrons;[36] a is a parameter, which equals 0.1542; $m^{3{\rm d}}$ is the number of magnetic electrons; $C = 0.907P$, with P being a constant related to the element group; W is the ratio of the sum of magnetic electrons and dumb-pair electrons to the total electrons. The detailed calculations of these parameters can be found in Ref. [29]. The hybrid tables of Cu, Sm, In, Te are shown in Tables A1–A4 in Appendix A. The A-type hybrid of Cu without 3d magnetic electron is selected for calculating the valence electron structure since $CuIn_{1-x}Sm_xTe_2$ is nonmagnetic material. The B-type table of Cu is magnetic at h state.

3. Results and discussion

Figure 1 shows the structural frame of $CuIn_{1-x}Sm_xTe_2$, which is built based on the refined structural parameters.[37] The experimental bond lengths are measured based on the atomic ordinates and the numbers of equivalent bonds I_α are calculated based on the atomic coordination numbers. Table 1 lists the experimental bond lengths and numbers of equivalent bonds in $CuIn_{1-x}Sm_xTe_2$. The valence electron structures of $CuIn_{1-x}Sm_xTe_2$ are calculated by the BLD method. The $CuInTe_2$ is chosen as an example, and its equivalent bonds I_α, *i.e.*, experimental and calculated bond lengths are listed in Table 2. The maximum of covalent electron pair n_A is 1.4628, thus, β is 0.71 according to Eq. (4). The calculated bond lengths fit to the experimental ones well ($\Delta D = -0.0070$ Å), showing that the calculated results are acceptable.

The key parameters of cohesive energy of $CuIn_{1-x}Sm_xTe_2$ are listed in Table 3. The shielding coefficient b value is 20.6044 kcal·Å/mol for Cu, 32.894 kcal·Å/mol for In, 37.500 kcal·Å/mol for Te, and 45.7317 kcal·Å/mol for Sm. The P value is 0 for IB group (Cu), IIIB group (Sm), and A group (In and Te); f and f' will change in various ranges.

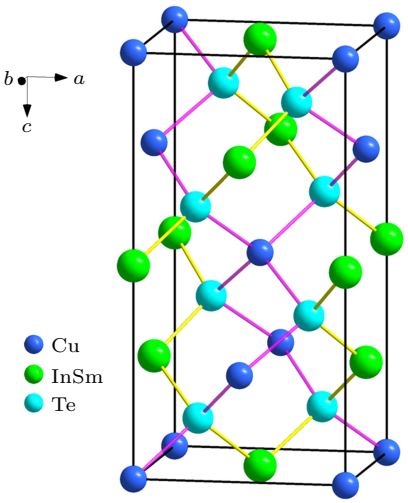


Fig. 1. Crystal structure of $CuIn_{1-x}Sm_xTe_2$.

Table 1. Various bonds, bond lengths, and bond numbers of $CuIn_{1-x}Sm_xTe_2$.

Compounds	Bond order	Bonding atom	I_α	Bond length (Å)	Bond order	Bonding atom	I_α	Bond length (Å)
$CuInTe_2$	1	Cu–Te	8	2.5797	6	Cu–In	8	4.3822
	2	In-Te	8	2.7943	7	Cu–Cu	4	4.3822
	3	Te–Te	4	4.1227	8	In-In	4	4.3822
	4	Te–Te	8	4.2568	9	Te–Te	8	4.5196
	5	Cu–In	8	4.3777	10	Te–Te	4	4.6486
$CuIn_{0.9}Sm_{0.1}Te_2$	1	Cu–Te	8	2.5816	6	Cu–In, Sm	8	4.3836
	2	In, Sm–Te	8	2.7941	7	Cu–Cu	4	4.3836
	3	Te–Te	4	4.1271	8	In, Sm–In, Sm	4	4.3836
	4	Te–Te	8	4.2593	9	Te–Te	8	4.5195
	5	Cu–In, Sm	8	4.3797	10	Te–Te	4	4.6479
$CuIn_{0.8}Sm_{0.2}Te_2$	1	Cu–Te	8	2.5825	6	Cu–In, Sm	8	4.3805
	2	In, Sm–Te	8	2.7889	7	Cu–Cu	4	4.3805
	3	Te–Te	4	4.1312	8	In, Sm–In, Sm	4	4.3805
	4	Te–Te	8	4.2597	9	Te–Te	8	4.5124
	5	Cu–In, Sm	8	4.3766	10	Te–Te	4	4.6368
$CuIn_{0.7}Sm_{0.3}Te_2$	1	Cu–Te	8	2.5800	6	Cu–In, Sm	8	4.3825
	2	In, Sm-Te	8	2.7941	7	Cu–Cu	4	4.3825
	3	Te–Te	4	4.1234	8	In, Sm–In, Sm	4	4.3825
	4	Te–Te	8	4.2573	9	Te–Te	8	4.5195
	5	Cu–In, Sm	8	4.3778	10	Te–Te	4	4.6481

Table 2. Valence electronic structure of $CuInTe_2$.

$I\alpha$	$\overline{D}_{uv}(n_\alpha)$ (Å)	$D_{uv}(n_\alpha)$ (Å)	ΔD (Å)	n_α	$\Delta D/D_{uv}(n_\alpha)$ (%)
8	2.5727	2.5797	–0.0070	1.4628	–0.2713
8	2.7873	2.7943	–0.0070	0.3392	–0.2505
4	4.1158	4.1228	–0.0070	0.0080	–0.1698
8	4.2498	4.2568	–0.0070	0.0052	–0.1644
8	4.3707	4.3777	–0.0070	0.0025	–0.1599
8	4.3752	4.3822	–0.0070	0.0024	–0.1597
4	4.3752	4.3822	–0.0070	0.0011	–0.1597
4	4.3752	4.3822	–0.0070	0.0052	–0.1597
8	4.5126	4.5196	–0.0070	0.0022	–0.1549
4	4.6416	4.6486	–0.0070	0.0014	–0.1506

Table 3. Key parameters of cohesive energy for $CuIn_{1-x}Sm_xTe_2$.

Element	b (kcal·Å/mol)	F	f'	P
Cu	20.6044	2.0000–2.0702	0.6325–0.5345	0
In	32.8940	1.4142–3.1389	0.8165–0.0000	0
Sm	45.7317	3.1947–3.6811	0.8165–0.0000	0
Te	37.5000	1.9319–1.7321	0	0

Table 4. Hybrid states and hybrid energy of $CuIn_{1-x}Sm_xTe_2$.

Compounds	σ	Cu	In	Te	Sm	Hybrid energy (eV)
$CuInTe_2$	1	9	10	1	–	13.6432
	2	11	10	1	–	13.7978
	3	17	9	1	–	13.8729
	4	13	10	1	–	14.8681
	5	17	10	1	–	15.3614
$CuIn_{0.9}Sm_{0.1}Te_2$	1	13	9	1	1	13.2397
	2	11	10	1	1	13.4953
	3	15	9	1	1	13.5668
	4	13	10	1	1	14.5603
	5	15	10	1	1	14.8979
$CuIn_{0.8}Sm_{0.2}Te_2$	1	13	9	1	1	12.7769
	2	11	10	1	1	12.9008
	3	13	10	1	1	13.9581
	4	15	10	1	1	14.2933
	5	17	10	1	1	14.4455
$CuIn_{0.7}Sm_{0.3}Te_2$	1	9	10	1	1	12.3834
	2	13	9	1	1	12.5614
	3	13	10	1	1	13.5853
	4	15	10	1	1	13.9182
	5	17	10	1	1	14.0697

According to the above-mentioned valence electronic structural parameters, all hybridization energy levels of $CuIn_{1-x}Sm_xTe_2$ are calculated from Eq. (11), and their results are listed in Table 4. The valence electronic structure of $CuIn_{1-x}Sm_xTe_2$ shows that the hybrid states of Te and Sm are close to the h state, however, Cu and In prefer to occupy the high hybrid state, which are closes to the t state. The hybridization energy decreases with Sm content increasing.

The light absorption causes the energy level to transit from the static state to the high energy state in $CuIn_{1-x}Sm_xTe_2$ as shown in Fig. 2. The transitions are from the 3rd energy level to the 4th energy level for $CuInTe_2$ and from the 1st to 5th energy level for the other ones. The energy difference between the two energy levels matches the experimental absorption bandgap of $CuIn_{1-x}Sm_xTe_2$ [37] with the relative differences ranging from 1.290% to 6.108% as listed in Table 5. Based on the valence electron structure, the light absorption mainly affects the hybrid states of Cu and In atoms as shown in Fig. 3, where the solid blue line and dashed red line denote the energy before (static state) and after (excited state) light absorption, respectively. The difference in energy between the two states is corresponding to the light absorption bandgap. It is very clear that the hybridization energy of $CuIn_{1-x}Sm_xTe_2$ decreases significantly with the increase of Sm doped into $CuInTe_2$ before and after light absorption. However, the decreasing slope slowly falls down after light absorption, which causes the light absorption bandgap to broaden from 0.9952 eV to 1.6862 eV with Sm content increasing: this phenomenon might be due to the special valence electron structure of Sm, which is favorable for enhancing the light absorption in a wider range for the potential solar cell applications.

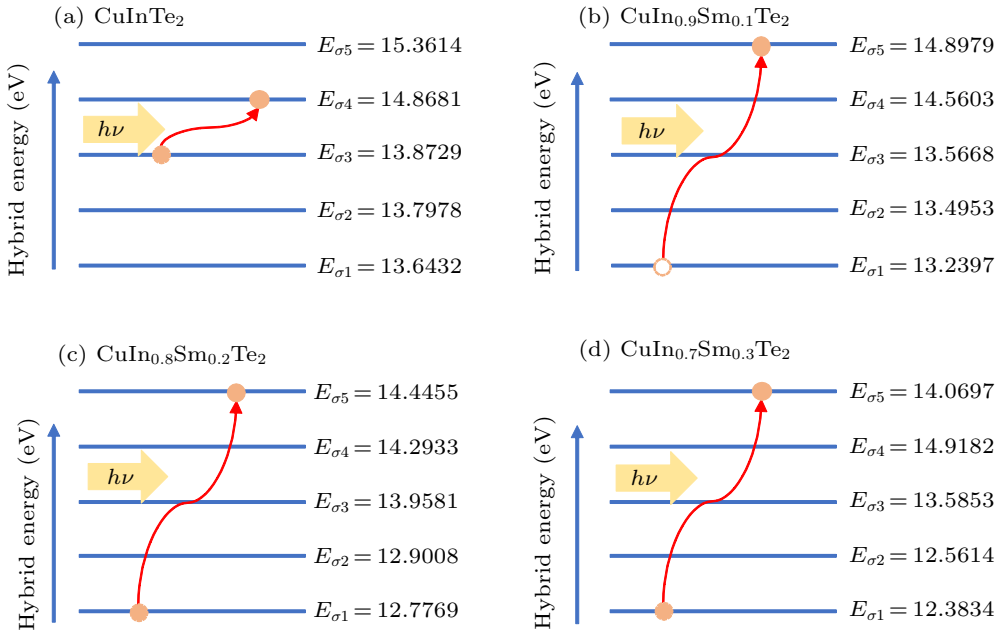


Fig. 2. Optical transition energy from static energy level to excited energy level in $CuIn_{1-x}Sm_xTe_2$.

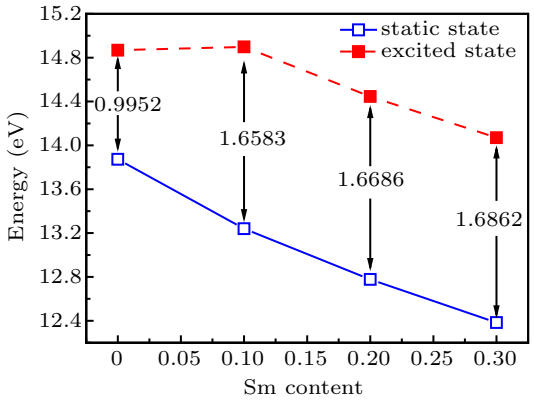


Fig. 3. Hybridization energy *versus* Sm content for $CuIn_{1-x}Sm_xTe_2$ in static state (solid line) and excited state (dashed line).

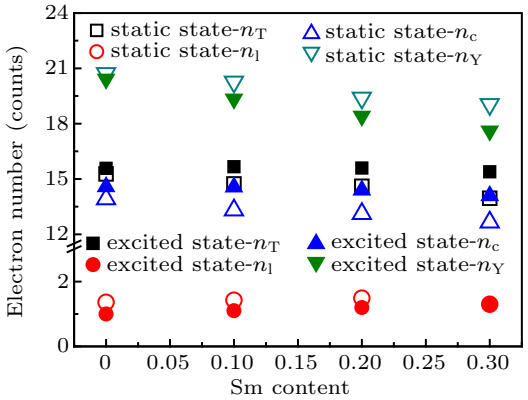


Fig. 4. Various electron numbers *versus* Sm content for $CuIn_{1-x}Sm_xTe_2$ in static state and excited state.

Table 5. Hybrid states, energy, and light absorption bandgaps of $CuIn_{1-x}Sm_xTe_2$.

Compounds	σ	Cu	In	Te	Sm	Hybrid energy (eV)	Energy difference (eV)	Bandgap (eV)	Fitting error
$CuInTe_2$	4	13	10	1		14.8681	0.9952	1.0600	0.06108
	3	17	9	1		13.8729			
$CuIn_{0.9}Sm_{0.1}Te_2$	5	15	10	1	1	14.8979	1.6583	1.6799	0.01290
	1	13	9	1	1	13.2397			
$CuIn_{0.8}Sm_{0.2}Te_2$	5	17	10	1	1	14.4455	1.6686	1.6999	0.01843
	1	13	9	1	1	12.7769			
$CuIn_{0.7}Sm_{0.3}Te_2$	5	17	10	1	1	14.0697	1.6862	1.5999	0.05393
	1	9	10	1	1	12.3834			

Table 6. Valence electron structures of $CuIn_{1-x}Sm_xTe_2$ in static and excited states.

Compounds	State	Atom	σ	n_s	n_p	n_d	n_c	n_l	n_m	n_Y
$CuInTe_2$	static state	Cu	17		2.9958	2.9958	5.9916	1		4.0084
		In	9	0.6399	2.6399	0.6399	3.9197	0.3601		8.7202
		Te	1	1	1	0	2	0	0	4
		Sm	–							
	excited state	Cu	13		2.7887	2.7887	5.5774	1		4.4226
		In	10	1	3	1	5			8
		Te	1	1	1	0	2	0	0	4
		Sm	–							
$CuIn_{0.9}Sm_{0.1}Te_2$	static state	Cu	13		2.7887	2.7887	5.5774	1		4.4226
		In	9	0.6399	2.6399	0.6399	3.9197	0.3601		8.7202
		Te	1	1	1	0	2	0	0	4
		Sm	1		1	1	2	1	0	0
	excited state	Cu	15		2.9310	2.9310	5.8620	1		4.1380
		In	10	1	3	1	5			8
		Te	1	1	1	0	2	0	0	4
		Sm	1		1	1	2	1	0	0
$CuIn_{0.8}Sm_{0.2}Te_2$	static state	Cu	13		2.7887	2.7887	5.5774	1		4.4226
		In	9	0.6399	2.6399	0.6399	3.9197	0.3601		8.7202
		Te	1	1	1	0	2	0	0	4
		Sm	1		1	1	2	1	0	0
	excited state	Cu	17		2.9958	2.9958	5.9916	1		4.0084
		In	10	1	3	1	5			8
		Te	1	1	1	0	2	0	0	4
		Sm	1		1	1	2	1	0	0
$CuIn_{0.7}Sm_{0.3}Te_2$	static state	Cu	9		2.2752	2.2752	4.5504	1		5.4496
		In	10	1	3	1	5			8
		Te	1	1	1	0	2	0	0	4
		Sm	1		1	1	2	1	0	0
	excited state	Cu	17		2.9958	2.9958	5.9916	1		4.0084
		In	11	1	3	1	5			8
		Te	1	1	1	0	2	0	0	4
		Sm	1		1	1	2	1	0	0

Table 6 lists the valence electron structures of $CuIn_{1-x}Sm_xTe_2$ at static states and excited states, covering the numbers of various electrons. Sm doped into $CuInTe_2$ mainly affects the hybrid states of Cu and In, and causes various electrons to change as shown in Fig. 4. In the static state, the electron numbers significantly fall down for dumb-pair electron n_Y, covalent electron n_c and total electron n_T with Sm doping content increasing, however, for the number of lattice electrons n_l increases. The same phenomenon is also observed in the excited state; however, the decreasing tendency of total electron number tends to be slow. With the decrease of hybridization energy, the total electron number (n_T) decreases from 15.2714 to 13.9503 and from 15.5773 to 15.3916 before and after light absorption, respectively, and the same tendency is also observed in covalent electron number (n_c) from 13.9113 to 12.6503 for the static state and from 14.5774 to 14.0916 for the light absorption, the dumb-pair electron number (n_Y) decreases from 20.7285 to 19.0497 and from 20.4226 to 17.6083 before and after light absorption, respectively. However, the lattice electron number shows the reversal tendency, *i.e.*, it increases from 1.3601 to 1.4881 and from 1.0000 to 1.3000 before and after light absorption, respectively. The abnormal decrease of n_l is observed in $CuIn_{0.7}Sm_{0.3}Te_2$ since the Sm content is out of the solid solution region of $CuIn_{1-x}Sm_xTe_2$. These changes of valence electronic structure weaken the bonding ability due to the decrease of covalent electron number and induce the hybrid energy of $CuIn_{1-x}Sm_xTe_2$ to decrease with Sm doping content increasing.

Figure 5 exhibits the changes of valence electron structure in $CuIn_{1-x}Sm_xTe_2$ before and after light absorption. The differences in electron number Δn_{ele} reflect the changes of valence electron number in s, p, and d orbits, the covalent electrons, lattice electrons, total electrons, and dumb-pair electrons before and after light absorption. The value of Δn_{ele}s increases for the total electron number and the covalent electron number, however, decreases for the dumb-pair electron number and the lattice electron number, which is due to the electron transformation driven by light energy. For revealing the mechanism of light absorption, the optical transition energy between two hybrid energy levels is discussed as shown in the inset plots in Fig. 5, where the photoenergy directly drives the electron transformation from lattice electron in static energy state to s valent electron in excited energy. Meanwhile, the dumb-pair electrons are separated from a dumb-pair of electrons in static state to two valence electrons in p and d orbitals in excited state. In a range of $x > 0.2$, the electron transition only occurs for the dumb-pair electrons because $CuIn_{1-x}Sm_xTe_2$ ($x = 0.3$) is out of the solid solution.

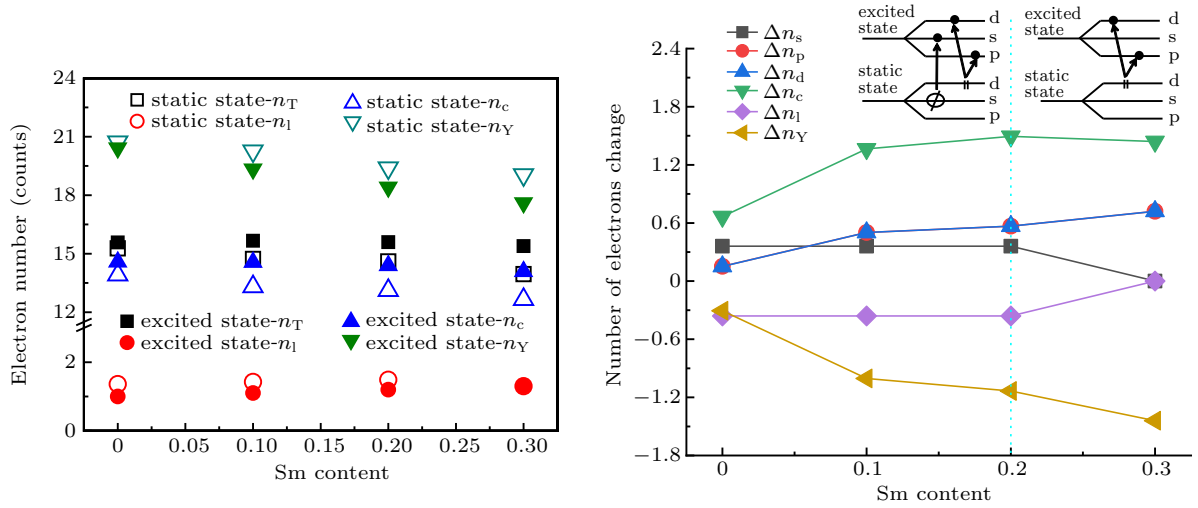


Fig. 5. Differences in electron number *versus* Sm content for $CuIn_{1-x}Sm_xTe_2$ after light absorption.

4. Conclusions

Based on EET studies, the cohesive energy of Sm doped into $CuInTe_2$ is strongly correlative to their valence electronic structure. The cohesive energy of $CuIn_{1-x}Sm_xTe_2$ decreases significantly with the increase of Sm doped into $CuInTe_2$ before and after light absorption. The light absorption causes the energy level to transit from the static state to the high energy in $CuIn_{1-x}Sm_xTe_2$. The calculated optical absorption transition energy from the static state to the higher energy in $CuIn_{1-x}Sm_xTe_2$ accords well with the experimental absorption bandgap of $CuIn_{1-x}Sm_xTe_2$. The Sm doped into $CuInTe_2$ mainly affects the electric structure of Cu and the electric structure of In, and the electron number of $CuIn_{1-x}Sm_xTe_2$ significantly falls down for dumb-pair electron n_Y, covalent electron n_c, and electron n_T with the increase of Sm doping content, however, the reversal increase happens to the number of lattice electrons n_l, which weakens the bonding ability due to the decrease of covalent electron number and induce the the hybrid energy of $CuIn_{1-x}Sm_xTe_2$ to decrease.

The mechanism of light absorption for $CuIn_{1-x}Sm_xTe_2$ can be explained by photoenergy driving directly the electron transformation from lattice electron in static energy level to s valent electron in excited energy level. Meanwhile, the dumb-pair electrons are separated from a pair of electrons to two electrons and excited into p, d orbitals of excited state, respectively. The energy bandgap of $CuIn_{1-x}Sm_xTe_2$ is significantly widened with increasing Sm content due to its special valence electron structure, which is favorable for enhancing the light absorption in a wider range for the potential applications in solar cells.

Appendix A: The hybrid tables of Cu, Sm, In, and Te

The hybrid tables of Cu, Sm, In, and Te are shown in the following tables.

Table A1. A-type hybrid table of Cu.

h ‖ ‖ ‖ • • ⏀ • • ○ 1 2 2 0
l ‖ ‖ • • • ⏀ • • • 1 3 3 0

σ	1	2	3	4	5	6	7	8	9
$C_h\sigma$	1	0.9999	0.9998	0.9983	0.9752	0.9502	0.9415	0.7997	07248
Ctσ		0.0001	0.0002	0.0017	0.0248	0.0498	0.0585	0.2003	0.2752
$n_T\sigma$	5	5.0002	5.0004	5.0034	5.0496	5.0996	5.1170	5.4006	5.5504
$n_l\sigma$	1	1	1	1	1	1	1	1	1
$n_c\sigma$	4	4.0002	4.0004	4.0034	5.0496	4.0996	4.1170	4.4006	4.5504
$R\sigma(1)$	1.1520	1.1520	1.1520	1.1520	1.1517	1.1513	1.1512	1.1492	1.1481
σ	10	11	12	13	14	15	16	17	18
$C_h\sigma$	0.6896	0.6601	0.5194	0.2113	0.1297	0.0690	0.0075	0.0042	0
Ctσ	0.3104	0.3399	0.4806	0.7887	0.8703	0.9310	0.9925	0.9958	1
$n_T\sigma$	5.6208	5.6798	5.9612	6.5774	6.7406	6.8620	6.9850	6.9916	7
$n_l\sigma$	1	1	1	1	1	1	1	1	1
$n_c\sigma$	4.6208	4.6798	4.9612	5.5774	5.7406	5.8620	5.9850	5.9916	6
$R\sigma(1)$	1.1477	1.1472	1.1453	1.1410	1.1398	1.1390	1.1381	1.1381	1.1380

Table A2. Hybrid table of In.

h ‖ ‖ ‖ ‖ ‖ ⏀ • • ○ 1 2 0 0
t ‖ ‖ ‖ ‖ • • • • 1 3 1 1

σ	1	2	3	4	5	6	7	8	9	10
$C_h\sigma$	1	0.9996	0.9975	0.9755	0.8755	0.8735	0.7612	0.5495	0.3601	0
$C_t\sigma$		0.0004	0.0025	0.0245	0.1245	0.1265	0.2388	0.4505	0.6399	1
$n_T\sigma$	3	3.0008	3.0050	3.0490	3.2490	3.2530	3.4776	3.9010	4.2798	5
$n_l\sigma$	1	0.9996	0.9975	0.9755	0.8755	0.8735	0.7612	0.5495	0.3601	0
$n_c\sigma$	2	2.0012	2.0075	2.0735	2.3735	2.3795	2.7164	3.3515	3.9197	5
$R\sigma(1))$	1.4420	1.4420	4.4418	1.4404	1.4339	1.4338	1.4265	1.4127	1.4004	1.3770

Table A3. Hybrid table of Te.

h • ‖ ‖ • 1 1 0 1
t ‖ ‖ • • 0 2 0 1

σ	1	2	3	4
$C_h\sigma$ 1	0.5544	0.0820	1	
Ctσ 0	0.4456	0.9180	1	
$n_T\sigma$ 2	2	2	2	
$n_l\sigma$ 0	0	0	0	
$n_c\sigma$ 2	2	2	2	
$R\sigma(1)$	1.313	1.4194	1.531	1.550

Table A4. Hybrid table of Sm.

h • ○ ○ ○ ○ ⏀ • ○ ○ 1 1 1 0
t ○ ○ ○ ○ ○ • • • ○ 1 0 2 1

σ	1	2	3	4	5	6	7	8	9	10
$C_h\sigma$	1	0.9635	0.9042	0.8235	0.7078	0.6249	0.2996	0.2085	0.0444	0
$C_t\sigma$		0.0365	0.0958	0.1765	0.2922	0.3751	0.7004	0.7915	0.9556	1
$n_T\sigma$	3	3	3	3	3	3	3	3	3	3
$n_l\sigma$	1	0.9635	0.9042	0.8235	0.7078	0.6249	0.2996	0.20857	0.0444	0
$n_c\sigma$	2	2.0365	2.0958	2.1765	2.2922	2.3751	2.7004	2.7915	2.9556	3
$R\sigma(1)$	1.4771	1.4901	1.5112	1.5398	1.5809	1.6104	1.7260	1.7584	1.8166	1.8325

References

[1] Chiker F, Abbar B, Tadjer A, Bresson S, Khelifa B and Mathieu C 2004 *Physica B: Condens. Matter* **349** 181
[2] Kopytov A V and Kosobutsky A V 2009 *Phys. Solid State* **51** 2115
[3] Sahin S, Ciftci Y O, Colakoglu K and Korozlu N 2012 *J. Alloys Compd.* **529** 1
[4] Liu H T, Xu C M, Sun Y, Li F Y, Zhang L, Xue Y M and He Q 2007 *Chin. Phys. B* **16** 788
[5] Tang F L, Liu R, Xue H T, Lu W J, Feng Y D, Rui Z Y and Huang M 2014 *Chin. Phys. B* **23** 077301
[6] Wang T, Guo Y Q, Wang C and Yang S W 2020 *J. Magn. Magn. Mater.* **502** 166506
[7] Bodnar I V, Gurin V S, Solovei N P and Molochko A P 2007 *Semiconductors* **41** 939
[8] Fu L and Guo Y Q 2014 *Chin. Phys. B* **23** 127801
[9] Mobarak M and Shaban H T 2014 *Mater. Chem. Phys.* **147** 439
[10] Jackson P, Wuerz R, Hariskos D, Lotter E, Witte W and Powalla M 2016 *Phys. Status Solidi* **10** 583
[11] Yang K J, Son D H, Sung S J, Sim J H, Kim Y I, Park S N, Jeon D H, Kim J, Hwang D K, Jeon C W, Nam D, Cheong H, Kang J K and Kim D H 2016 *J. Mater. Chem. A* **4** 10151
[12] Nie X M and Guo Y Q 2015 *J. Solid State Chem.* **233** 211
[13] Li S and Guo Y Q 2016 *Presented at the* 2*nd Annual International Conference on Advanced Material Engineering* (AME 2016), (unpublished)
[14] Wang T, Han J P and Guo Y Q 2017 *Advanced Materials and Energy Sustainability*, eds. Chen J I and Li Q (Singapore: Word Scientific) pp. 150–155
[15] Wang T, Guo Y Q and Li S 2017 *Chin. Phys. B* **26** 103101
[16] Mitzi D B, Copel M and Murray C E 2006 *Adv. Mater.* **18** 2448
[17] Shahroosvand H and Ghorbani-Asl M 2013 *J. Lumin.* **144** 223
[18] Arai T, Timmerman D, Wakamatsu R, Lee D G and Koizumi A 2015 *J. Lumin.* **158** 70
[19] Lü Z J and Wang S K 1979 *Chin. Sci. Bull.* **24** 742
[20] Guo Y Q, Yü R H, Zhang R, Zhang X and Tao K 1998 *J. Phys. Chem. B* **102** 9
[21] Li Z, Xu H and Gong S 2004 *J. Phys. Chem. B* **108** 15165
[22] Wu W X, Guo Y Q, Li A H and Li W 2008 *Acta Phys. Sin.* **57** 2486 (in Chinese)
[23] Zhang R L, Wu S and Yü R L 1988 *Sci. China Ser. A* **31** 1487
[24] Liu Z L, Li Z L and Liu W D 2001 *Sci. China Ser. E* **44** 542
[25] Guo Y Q, Su T, Zhang J, Wang X Q, Chen Y and Zhao X 2020 *ACS Appl. Energy Mater.* **3** 5361
[26] Zhang A M, Zhao Z, Yin G and Lin C 2017 *Comput. Mater. Sci.* **140** 61
[27] Li S, Zhao D, Wang H, Zhang Y, Huang W and Zhou Y 2020 *Mater. Chem. Phys.* **249**
[28] Yü R H 1978 *Chin. Sci. Bull.* **23** 217
[29] Zhang R L 1993 *The Empirical Electron Theory of Solids and Molecules* (Changchun: Jilin Science and Technology Press) (in Chinese)
[30] Elizalde-Galindo J T, Rivera Gómez F J, Matutes-Aquino J A and Botez C E 2008 *J. Magn. Magn. Mater.* **320** e58
[31] Meng Z H, Fu L, Mei J and Guo Y Q 2013 *Scientia Sinica Physica, Mechanica & Astronomica* **43** 275
[32] Meng Z H, Li J B, Guo Y Q and Wang Y 2012 *Acta Phys. Sin.* **61** 107101 (in Chinese)
[33] Wang S K and Lv Z J 1981 *Chin. Sci. Bull.* **26** 217
[34] Qian C F, Chen X F, Yü R H, Gend P and Duan Z Q 1997 *Sci. China Ser. A* **40** 308
[35] Lin C, Huang S X, Yin G L, Zhang A M, Zhao Z W and Zhao Y Q 2016 *Comput. Mater. Sci.* **123** 263
[36] Bhattacharya R N and Rajeshwar K 1986 *Solar Cell* **16** 237
[37] Nie X M and Guo Y Q 2015 *Adv. Mater. Res.* **1094** 218